Molecular Dynamics Simulation of Reactive Compatibilization of Polymer Blends

Chuck Yeung* and Kimberly A. Herrmann

School of Science, The Pennsylvania State University at Erie, Erie, Pennsylvania 16563-0203

Received July 30, 2002; Revised Manuscript Received October 28, 2002

ABSTRACT: Molecular dynamics simulations of reactive compatibilization of polymer blends are performed for a wide range of chain lengths and densities of reactive groups ρ_o. We directly observe the predicted diffusive growth as well as the saturation at later times. The crossover to the saturation regime is consistent with theoretical predictions. There is also a separate transition from second to first-order reaction kinetics. However, the crossover to first-order kinetics does not agree with predictions. Although a depletion layer builds up on a time scale $\propto \rho_o^{-2}$, we find that, for times less than the Rouse time τ_g, the copolymer per area is a function only of $t\rho_o^3$ for a wide range of ρ_o implying an additional crossover time scale which scales as ρ_o^{-3}. The interface is unstable at later times for sufficiently large ρ_o. The surface tension vanishes before the interface roughens showing that the instability is initiated mainly by the vanishing surface tension. The time required for the surface tension to vanish scales as ρ_o^{-3}. A dilute limit model is introduced to study the behavior for small ρ_o. In this limit, $\Sigma(t)$ grows linearly with time asymptotically and the reaction rate is a slowly decreasing function of Z in agreement with theoretical predictions. For times less than τ_g there is a logarithmic correction to the linear growth.

1. Introduction

Polymer blending is a cost-effective way to produce composites with desirable properties.[1−5] However, polymers are usually immiscible, so minority phase droplets often form large domains with weak adhesion to the matrix. To enhance the interfacial adhesion, copolymers can be added as compatibilizers. One way to accomplish this is via in situ copolymerization in which the polymers have complementary functional groups so they react at the interface to form a block copolymer layer.[6−9] The block copolymer layer enhances the mechanical blending of the polymers by lowering the surface tension[10−13] and inhibiting coalescence of minority phase droplets.[14,15] The copolymer layer also makes a mechanically stronger interface by forming entanglements between the copolymer layer and the homopolymer bulk phases.

Especially interesting results were obtained when polymers were end-functionalized with highly reactive end groups. When Orr et al. prepared a blend of aliphatic amine terminated polystyrene with anhydride terminated polyisoprene, they found that a microstructure on the order of hundreds of angstroms developed very quickly, much faster than predicted by mechanical mixing.[16] The experiment was repeated under static conditions to confirm that mixing was not crucial in the formation of the microstructure.[17] Jiao et al. observed that the interface roughened with increasing copolymer coverage and interpreted the instability as being due to vanishing of the surface tension.[18] Lyu et al., however, suggested that the instability is due both to the surface tension reduction and a kinetic mechanism generated by fluctuations induced on the interface.[17] O'Shaughnessy and Sawhney also argued that surface tension may be a secondary effect, at least for long chains, since the buildup of the copolymer layer will stop the grafting process before there is a significant reduction in the surface tension.[19,20]

Reactive compatibilization has only recently received theoretical attention.[19−26] The theoretical analysis usually assumes a planar interface between A and B homopolymer melts in which a fraction of the homopolymers are end-functionalized. In this paper, we will assume an unentangled, symmetric polymer blend with infinitely reactive end groups although in many situations the reaction kinetics are reaction controlled rather than diffusion control.[18,27,28] In our case, four distinct dynamical regimes are found theoretically for dilute reactants $\rho_o R_g^3 < 1$ where Z is the polymerization of the chains, ρ_o is the density of the reactive groups and R_g is the radius of gyration of the chains.

O'Shaughnessy and Vavylonis[23−25] discussed the reaction kinetics for times between the monomer diffusion time τ_a and the first Rouse time $\tau_g = 2R_g^2/(\pi^2 D)$, where D is the center of mass diffusion constant. In this time range the reaction kinetics is compact so that any two reactive ends initially within $x(t)$ of each other will have reacted within time t where $x(t) \sim t^{1/4}$ is the equilibrium root-mean-square displacement of the chain end in one direction. O'Shaughnessy and Vavylonis argued that the compact kinetics generates a depletion hole in the two point correlation function of the reactive ends and copolymer per area Σ grows as $\Sigma(t) \sim x(t)^4/\ln t$ or

$$\Sigma(t) = \rho_o^2 \frac{a^4 t}{\tau_a \ln(et/\tau_a)} \tau_a < t < \tau_g \qquad (1)$$

where a is the monomer size.

The kinetics for times greater than the Rouse time is discussed by both Fredrickson and Milner[21,22] and O'Shaughnessy and co-workers.[19,20,23−25] Both groups give similar results up to constant prefactors in the reaction rates and crossover times. Here we follow the discussion of Fredrickson and Milner. For times between the Rouse time τ_g and a crossover time τ_p, $\Sigma(t)$ is second order in ρ_o and grows linearly with time as

$$\Sigma(t) = K_o \rho_o^2 t = \frac{D}{K_o} \frac{t}{\tau_p}, \tau_g < t < \tau_p \qquad (2)$$

10.1021/ma021229x CCC: $25.00 © 2003 American Chemical Society
Published on Web 11/27/2002

where the effective rate constant is

$$K_o = \frac{101 D R_g^2}{\ln Z} \tag{3}$$

For unentangled chains, $K_o \sim 1/\ln Z$ since the diffusion constant $D \sim 1/Z$ while $R_g \sim Z^{1/2}$. The linear growth continues until all functional groups near the interface have reacted, thus forming a layer near the interface where reactive groups are depleted. The depletion layer forms on a time scale τ_p given by

$$\tau_p = \frac{D}{(K_o \rho_o)^2} \tag{4}$$

For times greater than τ_p, the polymers must diffuse through the depletion layer to react at the interface which then acts likes an absorbing surface. In this diffusive growth regime, $\Sigma(t)$ is first order in ρ_o and grows as

$$\Sigma(t) = \frac{2\rho_o}{\sqrt{\pi}}\sqrt{Dt} = \frac{2}{\sqrt{\pi}}\frac{D}{K_o}\sqrt{\frac{t}{\tau_p}}, \quad \tau_p < t < \tau_{sat} \tag{5}$$

Hence $\Sigma(t)$ is a function only of t/τ_p for $t < \tau_g$.

The reactions generate an increasingly dense layer of copolymers at the interface, causing the copolymers to be stretched perpendicular to the surface. The saturation layer is formed on a time scale τ_{sat} such that

$$\tau_{sat} = \frac{1}{D R_b^2 a^2 \rho_o^2} \tag{6}$$

The dense copolymer layer generates a chemical potential barrier to further polymers reaching the interface and the growth of Σ slows significantly with

$$\Sigma(t) = C_1\left(\ln\left[C_2\frac{t}{\tau_p}\right]\right)^{1/2}, \quad t > \tau_{sat} \tag{7}$$

where the constants C_1 and C_2 are given by

$$C_1 \approx \frac{1}{3aR_g}, \; C_2 = aR_g\frac{D}{K_o} \tag{8}$$

The predictions above are for the dilute case in which $\rho_o R_g^3 \ll 1$. For the semidilute case, where $\rho_o R_g^3 \gg 1$, Fredrickson and Milner[22] found similar results except there is a logarithmic correction to the linear growth regime and the new crossover times τ_p' and τ_{sat}' can be smaller than or of the same order as τ_g. O'Shaughnessy and Vavylonis found something similar but predicted an additional growth regime in which $\Sigma(t) \sim x(t) \sim t^{1/4}$ for $t < \tau_g$.[23,24]

Reactive compatibilization has been previously investigated numerically by Müller who used Monte Carlo simulations of the bond fluctuation model.[29] He varied the reactive density ρ_o at a single polymerization Z with $\rho_o R_g^3$ ranging from 0.041 to 0.1625. Although Müller was unable to observe the linear regime, he did see a small range of time where the data began to agree with predictions of the diffusive regime. He concluded that the linear regime could only be observed in simulations for simple molecules where $\rho_o R_g^3$ could be made sufficiently small. Yang and Char also used the bond-fluctuation model but were mainly interested in the effects of varying the number of reactive groups per polymer so did not focus on the different growth regimes.[30] O'Shaughnessy and Vavylonis performed numerical simulations using simple molecules which annihilated on contact and showed that there was indeed a transition from second-order to first-order reaction kinetics.[25]

In this paper, we present results of extensive molecular dynamics simulations of reactive compatibilization. Simulations are performed for chains with lengths ranging from $Z = 3$ to $Z = 40$ corresponding to unentangled Rouse dynamics. The reactive density is also varied through a wide range to explore the different dynamical regimes. Our data directly shows the diffusive regime in which $\Sigma(t) \sim t^{1/2}$ followed by a saturation regime in which $\Sigma(t)$ grows logarithmically slowly. The crossover between the diffusive and saturation growth regimes is consistent with theoretical predictions. There is also an additional transition from second order reaction kinetics at early times to first-order reaction kinetics during diffusive growth. A depletion layer builds up on a time scale $\tau_p \propto \rho_o^{-2}$ as predicted theoretically but the crossover from second order to first-order growth does not behave as predicted.

For times less than the Rouse time, we find that $\Sigma(t)$ is independent of chain length and depends only on ρ_o. This is expected since $\Sigma(t)$ only depends on the RMS chain end displacement $x(t)$ which is independent of Z for $t < \tau_g$. However, the scaling form is different from what is expected. We find that $\Sigma(t)$ can be written in the scaling form $\Sigma(t) = g(t(\rho_o a^3)^3)$ for a wide but finite range of ρ_o. This implies that, there is an additional crossover time scale which behaves as ρ_o^{-3} for this range of ρ_o.

The slope of the log−log plot of the early time ($t < \tau_p$) behavior of $\Sigma(t)$ increases toward one with decreasing reactive density, indicating that there may be a linear growth regime at very small ρ_o. However, this dilute limit cannot be accessed directly since it is extremely expensive computationally to obtain good statistics at small ρ_o. To investigate the $\rho_o \to 0$ limit, we introduce a dilute limit model in which we keep track of the number of unique pairs of chain ends that approach each other without actually linking the chains. Using this model, we observe an asymptotic linear growth regime and measure the asymptotic reaction rate constant K_o. We find that K_o is a slowly decreasing function of Z in agreement with theoretical predictions that $K_o \sim 1/\ln Z$. For $t < \tau_g$, we find that $\Sigma(t) \sim t/\ln t$, in agreement with the dilute limit prediction of O'Shaughnessy and Vavylonis.[24]

The interface is unstable and develops corrugations at late times for sufficiently large ρ_o. We track the surface tension as a function of time and find that the surface tension vanishes before the interface becomes unstable. Therefore, we conclude that the interfacial instability is initiated primarily by the vanishing surface tension rather than additional kinetic mechanisms. The time τ_σ required for the surface tension to vanish scales as $\tau_\sigma \sim \rho_o^{-3}$ for the range of ρ_o studied reflecting the ρ^{-3} scaling observed in the crossover from second to first-order reaction kinetics.

2. Simulation Method

We use a well-known polymer dynamics model developed by Grest, Kremer and co-workers[31−36] in which the monomers are in contact with a heat bath. The dynamics of the ith monomer is given by

$$\frac{d^2\mathbf{r}_i}{dt^2} = -\nabla_i U - \tilde{\Gamma}\frac{d\mathbf{r}}{dt} + \mathbf{w}_i(t) \quad (9)$$

Here distances are measured in terms σ and time in terms of $\tau = \sigma\sqrt{m/\epsilon}$ where m is the mass and σ and ϵ are the standard Lennard-Jones parameters. $\tilde{\Gamma} = \tau\Gamma$ where Γ is a microscopic friction constant which is independent of chain length and $\mathbf{w}$ is a Gaussian noise obeying

$$\langle w_{i,x}(t)\rangle = 0, \langle w_{i,x}(t)w_{j,x'}(t')\rangle = 2\tilde{\Gamma}\tilde{T}\delta_{x,x'}\delta_{ij}\delta(t-t') \quad (10)$$

with $\tilde{T} = k_B T/\epsilon$ where T is the temperature. The dimensionless interaction potential U consists of two parts $U = U_{LJ} + U_{anh}$ where U_{LJ} is the repulsive portion of the Lennard-Jones potential

$$U_{LJ} = 4\epsilon_{ij}\sum_{i<j}\left[\left(\frac{1}{r_{ij}}\right)^{12} - \left(\frac{1}{r_{ij}}\right)^{6} + \frac{1}{4}\right], \quad \text{for } r_{ij} < r_o \quad (11)$$

with $r_{ij} = |\mathbf{r}_i - \mathbf{r}_j|$ and $r_o = 2^{1/6}$. The energy parameters are $\epsilon_{AA} = \epsilon_{BB} = 1$ for monomers of the same type and $\epsilon_{AB} > 1$ for monomers of different type to induce phase separation. The polymer chain is held together by an additional anharmonic interaction U_{anh} between adjacent monomers on the same chain.

We used $\tilde{T} = 1$ and $\tilde{\Gamma} = 0.5$ with a monomer density of $\rho_{mon} = 0.85$ in our simulations. These parameters give results consistent with a polymer melt above the glass transition.[31] We chose $\epsilon_{AB} = 21$ to produce a strongly segregated polymer blend. Periodic boundary conditions were used in the y and z directions and anti-periodic boundary conditions were used in the x direction with the A−B interface lying on the $y-z$ plane.

The simulation is begun by placing the A polymers in one-half of the box and the B polymers in the other half. The system is then equilibrated without reactions until there is no systematic change in the thermodynamic and polymer statistics such as the pressure, surface tension, and polymer profiles. Equilibration times ranged from $t = 100$ for $Z = 3$ to $t = 2000$ for $Z = 40$. A fit of the equilibrium profile for $Z = 40$ to a tanh form gives a interfacial width of approximately 1.3. The reactions are turned on after the interface has equilibrated by randomly choosing a fraction f of the polymers to bear a single reactive end. When A and B reactive ends approach within r_o of each other the polymers are linked irreversibly via the same anharmonic potential which links adjacent monomers on a chain. Otherwise the reacted polymers obey the same dynamics as the nonreacted polymers.

Table 1 shows the important parameters in the simulations. Simulations were performed for chains of lengths $Z = 3$, 5, 10, 20, and 40 and with various reactive fractions f. The radius of gyration R_g and center-of-mass diffusion constant D are determined by simulating the equilibrated system without reactions. The first Rouse time $\tau_g = 2D/(\pi^2 R_g^2)$ is determined from the measured values of R_g and D. The data are noisier for early times and small ρ_o since few reactions have occurred. To compensate, more configurations are performed for shorter times and for smaller ρ_o to reduced the fractional uncertainty. Simulations for different system sizes were performed for $Z = 10$ and $Z = 20$ to check for finite size effects which were found to be minimal.

Kremer and Grest mapped this model to experimental data for polystyrene, polyethylene and other polymers.[31] They found that $\sigma \approx 1.2$ nm and $\tau = 3 \times 10^{-8}$ s for polystyrene and $\sigma \approx 0.5$ nm and $\tau \approx 7 \times 10^{-11}$ s for polyethylene. As an example our $Z = 40$ simulations would correspond to a system size of $52 \times 72 \times 72$ nm and a final time of 3.6×10^{-4} s for polystyrene and $20 \times 30 \times 30$ nm and 8.4×10^{-7} s for polyethylene.

3. Simulation Results

Figure 1 shows the copolymer per area $\Sigma(t)$ vs time for $Z = 20$. Results are shown for five different values of f from $f = 1/32$ to $f = 1$. The reactive density $\rho_o = f\rho_{mon}/Z$ varies correspondingly from $\rho_o = 0.00133$ to $\rho_o = 0.0425$. For $t < 0.2$, there is an approximately linear growth regime. This very early time regime occurs before the equilibrium end distribution is disturbed by the reactions. The reaction rate is just proportional to the equilibrium probability that two chain ends are in contact. This is a trivial linear regime that we ignore in the remainder of the paper. For the larger values of f, there is an intermediate diffusive growth regime where $\Sigma(t)$ grows approximately as $t^{1/2}$. For $f > 1/4$, there is an additional growth regime at late times in which the growth is much slower than diffusive, in general agreement with the theoretical predictions.

To provide a more quantitative test of the theoretical predictions, we follow Müller and plot the reaction rate in a scaled form.[29] Using eqs 2−7, we can define a scale reaction rate as

$$\tau_p\frac{d\Sigma}{dt} = \begin{cases} \dfrac{D}{K_o} & \tau_g < t < \tau_p \\ \dfrac{D}{\sqrt{\pi}K_o}\left(\dfrac{t}{\tau_p}\right)^{-1/2} & \tau_p < t < \tau_{sat} \\ C_1\dfrac{\tau_p}{2t}\dfrac{1}{\sqrt{\ln[C_2 t/\tau_p]}} & t < \tau_{sat} \end{cases} \quad (12)$$

Therefore, a plot of $\tau_p d\Sigma/dt$ vs t/τ_p should collapse on a single curve for all values of ρ_o.

Figure 2 shows this plot for $Z = 10$, $Z = 20$, and $Z = 40$ along with the theoretical predictions for the linear, diffusive and saturation growth regimes. For each Z, the curves for the different values of f all approach each other and approach the theoretical prediction for large scaled times t/τ_p. The only exception is the increase in $d\Sigma/dt$ at very late times for $Z = 10$, $f = 1$. This upturn is due to the instability of the interface as will be discussed later. Neglecting the effects of the instability, our results are in good agreement with the theoretical predictions when $t \gg \tau_p$. In particular, there is a clear diffusive growth regime in which $d\Sigma/dt \sim t^{-1/2}$ with an amplitude of the same order as predicted in eq 12. The diffusive growth is followed by a much slower saturation growth in which $d\Sigma/dt \sim 1/t$. The amplitude in the saturation regime is also in general agreement with the theoretical prediction. Plots of the copolymer density show that there is a region near the interface where the reactive ends are depleted and that the late time slower growth occurs when there is a significant density of copolymer at the interface. This behavior confirms the important physical mechanisms that determine the reaction kinetics in these regimes. The crossover time from the diffusive to saturation regimes is also in good agreement with the theoretical prediction given by eq 6. In particular $\tau_{sat} \sim \rho_o^{-2}$ and τ_{sat}/τ_p is of order 10^2.

Theoretically, the reaction dynamics is predicted to be second order at early times and first-order once a depletion layer develops. To test the order of the reaction kinetics, we plot $\Sigma(t)/\rho_o^2$ and $\Sigma(t)/\rho_o$ vs t for $Z = 20$ in Figures 3 and 4. Similar results are obtained for $Z = 10$ and $Z = 40$. The curves for the different values of f fall on top of one another at early times in the $\Sigma(t)/\rho_o^2$ vs t graph and approaches each other at late times in the $\Sigma(t)/\rho_o$ vs t graph. Hence, there is a transition from second-order reaction kinetics for $t \ll \tau_p$ to first-order reaction kinetics for $t \gg \tau_p$ as predicted theoretically and in agreement with simulations of simple molecules.[25,29]

Table 1. Simulation Parameters[a]

f	ρ_o	$\rho_o R_g^3$	τ_p	τ_{sat}	no. of configurations (time)
$Z = 3$, $D = 0.023$, $R_g = 0.67$, $\tau_g = 3.9$, $K_o = 0.70$, $l_x = 40$, $l_y = l_z = 60$, monomers = 122 400					
1	0.283	0.087	0.31	19.4	26 (100), 5 (2000)
$Z = 5$, $D = 0.015$, $R_g = 0.96$, $\tau_g = 13$, $K_o = 085$, $l_x = 40$, $l_y = l_z = 60$, monomers = 122 400					
1/2	0.085	0.076	2.84	251	10 (1000)
1	0.170	0.151	0.71	62.8	20 (4000)
$Z = 10$, $D = 0.0072$, $R_g = 1.48$, $\tau_g = 62$, $K_o = 0.69$, $l_x = 50$, $l_y = l_z = 60$, monomers = 153 000					
1/4	0.02125	0.069	34	4860	17 (400), 9 (8000)
1/2	0.0425	0.138	8.4	1220	10 (200), 6 (8000)
1	0.085	0.276	2.1	304	20 (100), 12 (4000), 4 (10000)
$Z = 20$, $D = 0.0032$,$R_g = 2.22$,$\tau_g = 310$, $K_o = 0.54$, $l_x = 40$, $l_y = l_z = 50$, monomers = 85 000					
1/32	0.00133	0.0145	6390	1.56×10^6	2352 (100), 560 (2000), 55 (4000)
1/16	0.00265	0.029	1600	3.89×10^5	1037 (100), 233 (2000), 142 (4000)
1/8	0.00532	0.058	400	97 300	394 (200), 34 (10000)
1/4	0.0106	0.116	100	24 300	165 (200), 26 (4000), 12 (12000)
1/2	0.02125	0.233	25	6100	86 (200), 16 (6000), 6 (12000)
1	0.0425	0.465	6.2	1520	67 (200), 43 (4000), 25 (12000)
$Z = 40$, $D = 0.0014$, $R_g = 3.25$, $\tau_g = 1560$, $K_o = 0.40$, $l_x = 40$, $l_y = l_z = 60$, monomers = 122 400					
1/8	0.00266	0.0946	1235	4.93×10^5	282 (400), 150 (2000)
1/4	0.00532	0.189	310	1.23×10^5	226 (200), 107 (400), 27 (4000)
1/2	0.01046	0.378	77	30 800	62 (200) 20 (12000)
1	0.02125	0.774	19	7710	71 (200) 20 (12000)

[a] See text for symbols. Number of configurations is the number of different initial configurations run to a given time. For example, for the $Z = 3$ case, 26 configurations are simulated up to at least $t = 100$ and 5 configurations are simulated up to $t = 2000$.

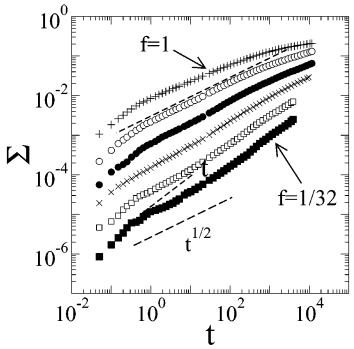

Figure 1. Copolymer per area $\Sigma(t)$ vs t for $Z = 20$ and reactive fraction $f = 1$ (+), $^1/_2$ (○), $^1/_4$ (●), $^1/_8$ (×), $^1/_{16}$ (□), and $^1/_{32}$ (■). Line showing diffusive $t^{1/2}$ and linear growth are drawn as guides to the eye.

The agreement with theory observed at late times is most likely because $\tau_{sat} \gg \tau_g$. For $t \gg \tau_g$, the polymers can be treated as simple molecules with effective size R_g and effective diffusion constant D. The agreement between the simulation and theory is not as good for $t \lesssim \tau_p$. Polymer connectivity effects are important in this time range since $\tau_p \lesssim \tau_g$ in most though not all of our simulations. Therefore, the theory for the semidilute case may be more appropriate. For example, for $Z = 20$, $f = {}^1/_2$, diffusive $t^{1/2}$ growth is observed even for $t < \tau_p$ as predicted by Fredrickson and Milner.[22] However, their analysis of the semidilute case predicts that the crossover time from the early to diffusive regime $\tau_p' = \tau_g (\rho_o R_g^3)^{-2}$ is larger than τ_g, so the semidilute theory does not predict $t^{1/2}$ growth for $t < \tau_p$ in our simulations.

In addition to not directly observing the linear growth regime, Figure 2 shows that the crossover to diffusive growth does not agree well with theoretical predictions; in particular, $\Sigma(t)$ is not a function only of t/τ_p except when $t \gg \tau_p$. The crossover time is predicted to scale as ρ_o^{-2} even for the semidilute case, so we still should observe a collapse of the scaled plots. This is probably because the theoretical arguments require a large separation between τ_g and τ_p which is not always true in our simulations.

To check that there is an underlying depletion time scale for the formation of the depletion layer that scales as ρ_o^{-2}, we calculate the integral

$$I(t) = \frac{1}{\rho_o^2} \int \mathrm{d}x\, \rho_{Ae}(x, t)\rho_{Be}(x, t) \qquad (13)$$

where $\rho_{Ae}(x)$ and $\rho_{Be}(x)$ are the density of reactive ends averaged over the y and z directions as a function of x. Figure 5 shows $I(t)$ and $\mathrm{d}\Sigma/\mathrm{d}t$ for $Z = 20$ plotted vs t/τ_p. Similar results are observed for $Z = 10$ and $Z = 40$. $I(t)$ decreases slowly at early times followed by a more rapid $t^{-1/2}$ decrease at later times. The decrease in $I(t)$, due to a decrease in reactive ends near the interface, is an indication of the formation of a depletion layer. The plots of $I(t)$ vs t/τ_p for the different values of ρ_o collapse onto each other, showing that the time required to form the depletion layer scales as ρ_o^{-2} as predicted theoretically. This characteristic time is of the same order as the theoretical prediction for τ_p since the more rapid decrease in $I(t)$ begins at $t \approx \tau_p$. However, it is surprising that the curves the plots for both $\tau_g > \tau_p$ and $\tau_g < \tau_p$ collapse onto a single master curve rather than two separate curves.

Within the mean field approximation, $I(t)$ is proportional to the scaled reaction rate $\tau_p \mathrm{d}\Sigma/\mathrm{d}t$. Figure 2 shows that this proportionality holds for $t \gg \tau_p$ but not at early times, $t \lesssim \tau_p$. The breakdown of the mean field prediction indicates that there is structure in the positions of the reactive ends along the interface. This is in agreement with the prediction that a depletion hole forms in the two-body correlation function at the interface as predicted by O'Shaughnessy and Vavylonis.[23,24] However, they also predict once the depletion layer forms $\Sigma(t) \sim x(t)$ even for $t < \tau_g$, which we do not observe.

Figure 2 shows that the crossover time from the early time second-order reaction kinetics to the first-order diffusive regime does not scale as ρ_o^{-2} as predicted. The question is, is there an alternative scaling for $t < \tau_g$. Figure 6 shows an attempt at an alternative scaling. Here we plot Σ vs $t(\rho_o a)^3$ for $Z = 10$, $Z = 20$ and $Z = 40$. Thirteen different data sets are shown with the value

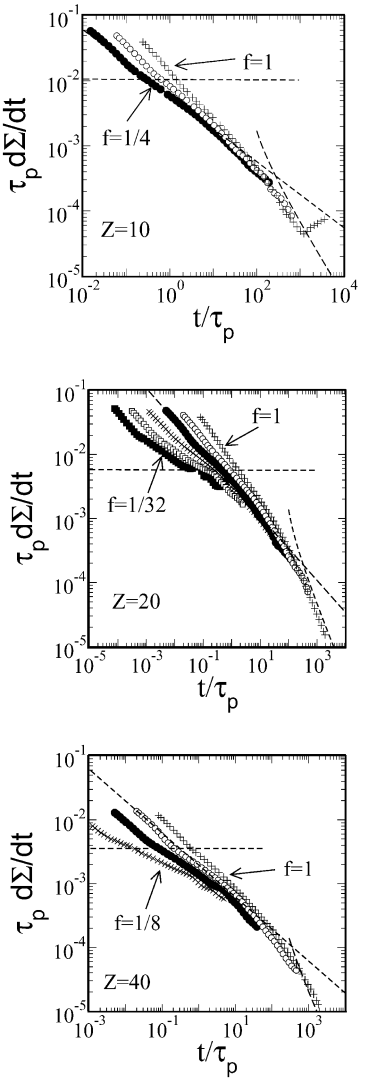

Figure 2. Scale reaction rate $\tau_p d\Sigma/dt$ vs t/τ_p for $Z = 10$, $Z = 20$, and $Z = 40$. The dashed lines show the theoretical predictions for the linear, diffusive, and saturation regimes. Symbols are the same as in Figure 1. The upturn in the reaction rate at late times for $Z = 10$, $f = 1$ occurs when the planar interface becomes unstable.

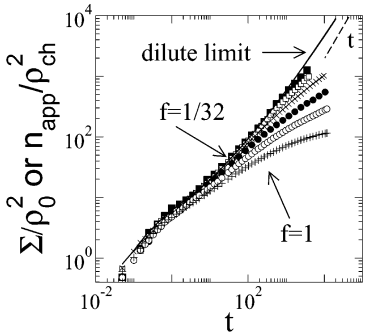

Figure 3. Copolymer per area $Z = 20$ scaled to test for second-order reaction kinetics (symbols) along with the results of the dilute limit model (solid line). Symbols are the same as in Figure 1. The collapse of the curves at early times indicates that the reaction kinetics are initially second order. The data for finite f approaches that of the dilute limit model as f is decreased. The dashed line shows that n_{app} grows linearly at late times.

of ρ_o varying by a factor of 64. Only data for $\tau_a < t < \tau_g$ is shown where $\tau_a \approx 15$ is the monomer diffusion time which we estimate by determining the time at which

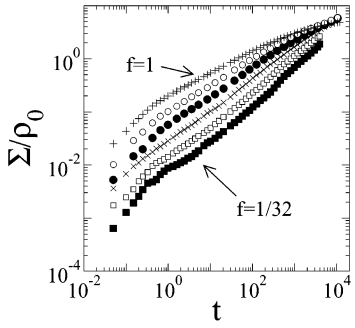

Figure 4. Copolymer per area for $Z = 20$ scaled to test for first-order reaction kinetics. Symbols are the same as in Figure 1. The curves for the different reactive fractions f approach each other at late times indicating first-order reaction kinetics.

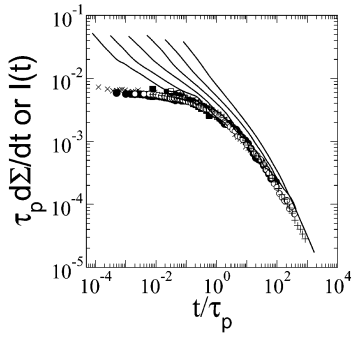

Figure 5. $I(t)$ (symbols) and $\tau_p d\Sigma/dt$ vst/τ_p (solid lines) for $Z = 20$. Symbols are the same as in Figure 1. The collapse of $I(t)$ indicates an underlying depletion crossover time that scales as ρ_o^{-2}. The difference in $I(t)$ and the scaled rate for $t \lesssim \tau_g$ indicates a breakdown in mean field theory.

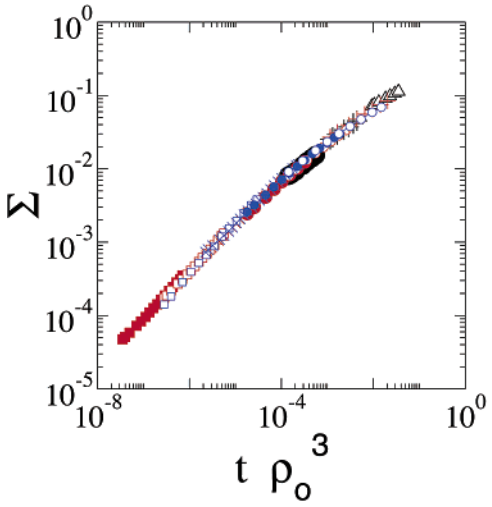

Figure 6. $\Sigma(t)$ for $Z = 10$ (black) $Z = 20$ (red), and $Z = 40$ (blue) plotted in an alternative scaling form vs $t(\rho_o a^3)^3$ for $\rho_o = 0.00133$ (■), 0.00265 (□), 0.00532 (x), 0.0106 (●), 0.0213 (○), 0.0425 (+) and 0.085 (▲). Only data for $\tau_a < t < \tau_g$ are shown for each Z. The different plots collapse onto a single master curve.

the RMS chain end displacement $x(t)$ is equal to 1. The data for different values of Z but the same ρ_o fall on top of one another. This is expected since $\Sigma(t)$ depends only on ρ_o and $x(t)$ which is independent of Z for $t < \tau_g$.

The data sets for different values of ρ_o seems to fall onto one master curve, indicating that $\Sigma(t)$ is a function only of $t(\rho_o)^3$, and there is a characteristic time that scales as $\tau' \sim \rho_o^{-3}$. Although this unexpected collapse is excellent, it probably only holds for a finite though large range of ρ_o. We know from Figure 5 that the

depletion layer forms on a time scale τ_p that scales as ρ_o^{-2}. For large ρ_o, this characteristic time scale is much smaller than τ_g and must affect the scaling behavior. This may be reflected in the fact that the overlap is not as good for the largest value of ρ_o shown in Figure 6.

We also ask whether the ρ_o^{-3} scaling holds for very small ρ_o. The second-order reaction kinetics for $t \ll \tau_p$ requires that, in the limit of $\rho_o \to 0$, $\Sigma(t) \sim t^{2/3}$ for $t < \tau_g$ if $\Sigma(t)$ is a function only of $t\rho_o^3$. As we will discuss in the next section, we know that $\Sigma(t) \sim t/\ln t$ for $t < \tau_g$ in the dilute reactant limit. Therefore, the ρ_o^{-3} scaling must breakdown for very small ρ_o. We conclude that we observe very good collapse of the data assuming a crossover time that scales as ρ_o^{-3} for a large range of ρ_o but that this range must be finite. However, we do not yet understand the physical origin of this scaling behavior.

4. Dilute Limit Model

Although we do not directly observe a regime in which $\Sigma(t)$ grows linearly, there are indications of such a regime in Figure 2. For $t < \tau_p$, the slope of the log−log plot of the reaction rate becomes shallower with decreasing ρ_o. Therefore, theoretical prediction of a constant reaction rate linear growth regime for $t \ll \tau_p$ may hold for very small values of ρ_o. However, we cannot investigate this dilute regime directly. This is because more and more configurations are needed to obtain useful statistics with decreasing ρ_o since very few reactions occur for each configuration. For example, we averaged over approximately 2400 configurations for $f = {}^1/_{32}$, $Z = 20$ corresponding to 200 million monomers. However, even with this expenditure of computational resources, the data are fairly noisy for this value of reactive density.

Therefore, rather than attempting to determine the linear reaction rate K_o by direct simulation of systems with very small ρ_o, we introduce a dilute limit model to investigate the dilute reactive density limit. For $t \ll \tau_p$, not enough reactions have occurred to affect the reactive group density profile near the interface nor are there enough copolymers at the interface to inhibit further reactions. Hence, in this limit, we can neglect the effect of the reactions after they occur. To take advantage of this, we run the simulation without reactions and count the first time different pairs of A−B ends approach each other. That is, when an A chain end approaches within r_o of a B end, we keep track of the index of the two polymers. We do not add to the count if the same two chains ends approach each other since they would not react again if both ends had been reactive. However, we do not link the two polymers since the probability that both ends are reactive is f^2 which is vanishingly small as $f \to 0$. After the approach we simply continue the simulation and add to our count if either of the chain ends approach a different chain end.

In this model, the number of unique approaches per area $n_{app}(t)$ can be related to the copolymer per area $\Sigma_f(t)$ for small f by $\Sigma_f(t) = f^2 n_{app}(t)$ or, since $\rho_o = f\rho_{ch}$ where ρ_{ch} is the number of chains per volume

$$\frac{n_{app}(t)}{\rho_{ch}^2} = \lim_{\rho_o \to 0} \frac{\Sigma_f(t)}{\rho_o^2} \tag{14}$$

To test the validity of the dilute limit model, Figure 3 shows $\Sigma_f(t)/\rho_o^2$ and $n_{app}(t)/\rho_{ch}^2$ vs time for $Z = 20$. For each value of f, $\Sigma_f(t)/\rho_o^2$ matches the dilute limit result

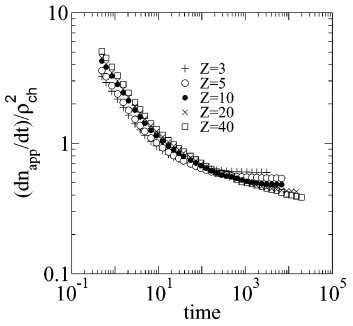

Figure 7. Reaction rate $\rho_{ch}^{-2} dn_{app}/dt$ in the dilute limit model for chains of length $Z = 3$, 5, 10, 20, and 40. The reaction rate approaches a constant value at late times which decreases slowly with chain length in agreement with theoretical predictions.

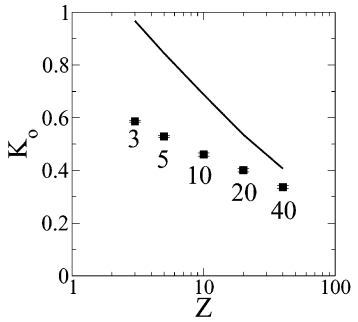

Figure 8. Asymptotic reaction rate K_o from the dilute limit model simulations along with the theoretical prediction (solid line). The data approaches the theoretical prediction with increasing Z. The uncertainty is smaller than the symbol size.

at early times and as f is decreased, the range of time in which $\Sigma_f(t)/\rho_o^2$ matches the dilute limit result increases. The figure also shows that n_{app} grows linearly with time for $t \gg \tau_g$. Therefore, we have confidence that the dilute limit model reproduces the physical result for small f and gives the linear reaction rate K_o. Furthermore, because the number of unique approaches is large, we do not need a large number of initial configurations to obtain high quality statistics. For example, for $Z = 20$, 24 configurations give a fractional uncertainty of 0.14% at $t = 20\,000$.

Figure 7 shows the effective reaction rate $K_{eff}(t) = \rho_{ch}^{-2} dn_{app}/dt$ for $Z = 3$, 5, 10, 20, and 40. For each Z, the reaction rate approaches a constant value at later times though there remains an observable curvature in the data for $Z = 20$ and $Z = 40$ at the latest times in the simulation. From the graph, the asymptotic reaction rate K_o decreases slowly with Z consistent with the theoretical prediction that asymptotic reaction rate $K_o \sim 1/\ln Z$. To provide a more quantitative comparison with theory, we obtain K_o by fitting $n_{app}(t)/\rho_{ch}^2$ for $t > 2\tau_g$ to the form $K_o t + B\sqrt{t} + C$ where B and C are constants. Different fitting forms gives similar values for K_o. The simulation results for K_o are given in Figure 8 along with the theoretical prediction of Fredrickson (eq 3).[21] The agreement between the experimental and numerical values becomes better with larger Z with the values of K_o at $Z = 40$ differing by about 15%. Therefore, our simulations of the dilute limit model confirm the theoretical predictions for the asymptotic linear reaction rate K_o for unentangled polymers at large Z and small ρ_o.

We can also examine the behavior for times less than the Rouse time. Equation 1 predicts that $\Sigma(t) = \rho_o^2 a^4/$

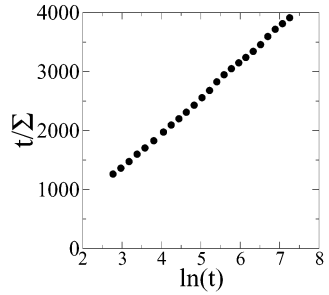

Figure 9. Plot of $t/\Sigma(t)$ vs ln t for $Z = 40$ and $\tau_a < t < \tau_g$. The linear dependence on ln t is consistent with the theoretical predictions but the amplitude is smaller than the theoretical prediction by about a factor of 25.

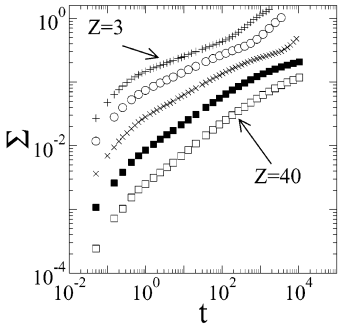

Figure 10. $\Sigma(t)$ for $Z = 3$ (+), $Z = 5$ (○), $Z = 10$ (×), $Z = 20$ (■), and $Z = 40$ (□) with all chains reactive ($f = 1$). The upturns in Σ at late times for $Z = 3$, 5, and 10 are due to the instability of the interface.

($\tau_a \ln(et/\tau_a)$) for $\tau_a < t < \tau_g$. Theoretically a plot of $t/\Sigma(t)$ vs ln t should give a straight line. Figure 9 shows the plot for $Z = 40$. Only the data between $\tau_a < t < \tau_g$ is shown. The figure shows that t/Σ is indeed linear in ln t as predicted theoretically, although the amplitude is smaller than the theoretical prediction by about a factor of 25. However, scaling arguments are used to obtain eq 1 so the difference is not unreasonable.[23]

5. Interfacial Instability

Figure 10 shows Σ vs t for the case in which all chains are reactive ($f = 1$). For the smaller values of Z ($Z = 3$, 5 and 10), there is an upturn in the Σ vs t plot at late times. This is due to the increase in surface area associated with the initially planar interface becoming unstable and roughening. This, in turn, generates a larger surface on which the polymers of different types can approach and react thereby increasing the reaction rate.

The instability is shown explicitly in Figure 11 for $Z = 10$, $f = 1$ in which a two-dimensional slice of the system is shown at different times. The copolymer layer grows until the entire interface is saturated with copolymers at $t \approx 1000$. The initially planar interface then becomes unstable and roughens by developing corrugations similar to those observed experimentally. These corrugations are expected once the interface is saturated with copolymers since the system enters a regime in which the two-homopolymer phases coexist with a swollen lamellar phase. The formation of the lamellar phase is what is observed at very long times experimentally.

An open question is whether the interfacial instability is initiated purely by the reduction of the surface tension with increasing copolymer coverage or if there are additional important dynamics effects. One propose

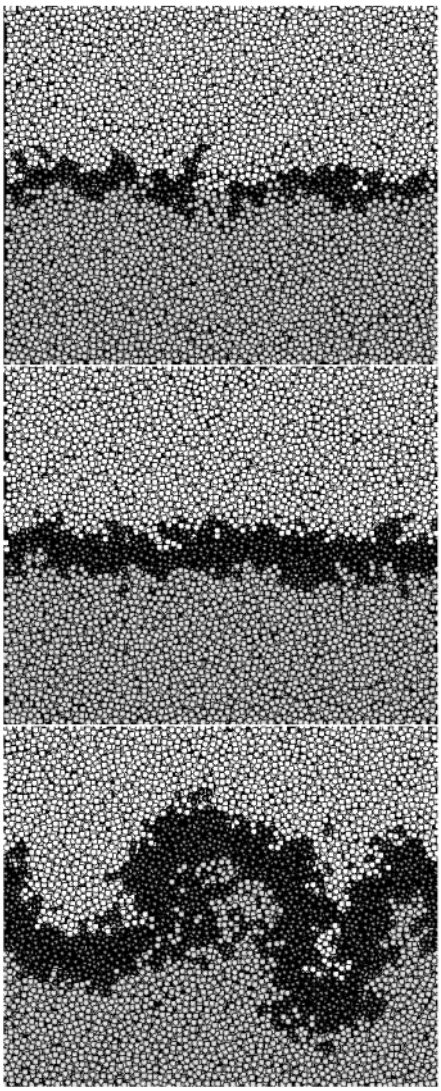

Figure 11. Two-dimensional slice of system for $Z = 10$ and $t = 100$, 1000, and 10000. The dark stripe in the middle is the copolymer layer. The surface tension vanishes at $t \approx 800$, but the interface remains essentially planar until $t \approx 4000$.

mechanism is that a deformation in the interface generates extra surface area for polymers to react and form copolymers. The extra surface area is then stabilized since the additional copolymer will prevent the surface from shrinking back to its original position. It is proposed that this mechanism can lead to an interfacial instability even without the surface tension completely vanishing.[17] To distinguish the two effects, we determine the interfacial surface tension by measuring the difference in the pressure perpendicular and tangential to the interface[35]

$$\sigma = l_x(P_x - P_{yz}) \tag{15}$$

where P_x is the pressure in the x direction, P_{yz} is the average of the pressure in the y, z directions and l_x is the x system size. Note that since the pressure different $P_x - P_{yz}$ is proportional to $1/l_x$, the surface tension is independent of system size l_x. Figure 12 shows the surface tension vs time for different chains lengths with all the chains reactive. Except for $Z = 40$, the surface tension vanishes before the end of the simulation and in fact becomes negative. The negative surface tension is thermodynamically unstable and the surface tension

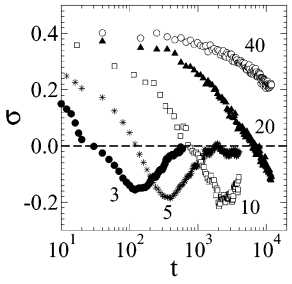

Figure 12. Surface tension σ as a function of time for $Z = 3$ (●), $Z = 5$ (∗), $Z = 10$ (□), $Z = 20$ (▲), and $Z = 40$ (○) and all chains reactive. The surface tension vanishes within the simulation time for all cases except $Z = 40$.

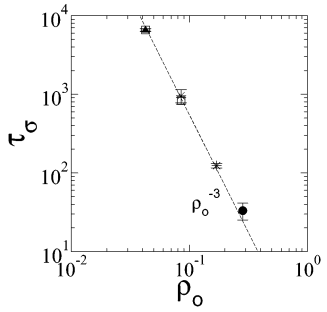

Figure 13. Time τ_σ required for the surface tension to vanish as a function of ρ_o for $Z = 3$ (●), $Z = 5$ (∗), $Z = 10$ (□), and $Z = 20$ (▲). For this limited range of values τ_σ is almost independent of the chain length and depends on ρ_o as $t_\sigma \sim \rho_o^{-3}$. This is consistent with the scaling observed for $t < \tau_g$.

returns to zero as the planar interface roughens, eliminating the anisotropy between the x and the y, z directions.

We note that eq 15 is a measure of the equilibrium surface tension but the system is not in equilibrium due to the ongoing reactions. To confirm that the nonequilibrium effects are not important in the surface tension measurement, we took some configurations in which the copolymers had already formed and continued the simulations without reactions. We found that the surface tension did not change after the reactions were turned off.

Comparisons of Figure 12 and Figure 10 and Figure 11 show that the surface tension vanishes before the upturn in $d\Sigma/dt$ and therefore the surface tension vanishes before interface becomes rough. (A very rough estimate shows that we observe the upturn in the $d\Sigma/dt$ at times which is a factor of 5−10 larger than the time at which the surface tension vanishes.) Hence, our results indicate that the main mechanism initiating the instability of the interface is the vanishing of the surface tension and not additional kinetic mechanisms since the surface tension vanishes first. However, kinetic mechanisms are important in determining when and how the interface roughens once the surface tension vanishes.

Figure 13 shows the time τ_σ required for the surface tension to vanish as a function of reactive density ρ_o for different chain lengths Z. Here data for $f < 1$ are also included. For this range of values, τ_σ depends primarily on ρ_o and is essentially independent of Z. As shown in the figure, $\tau_\sigma \sim \rho_o^{-3}$. This is consistent with the scaling that observed for $t < \tau_g$ shown in Figure 6. However, our data also indicates that the interface becomes saturated at a time $\tau_{sat} \propto \rho_o^{-2}$. Therefore, for very small ρ_o, $\tau_{sat} \ll \tau_\sigma$ and the growth in Σ should be severely suppressed before there is a significant reduction in the surface tension and no instability should be observed for very small ρ_o. Unfortunately, we cannot test this directly with our available computational resources.

6. Summary

Our molecular dynamics simulation of reactive compatibilization shows directly the presence of the predicted diffusive growth regimes in which the copolymer per area $\Sigma(t) \sim t^{1/2}$ as well as the late time saturation regime in which $\Sigma(t)$ grows logarithmically. The crossover time τ_{sat} is consistent with theoretical predictions. There is also a transition from an early time regime in which the reaction kinetics is second order in the reactive density ρ_o to the diffusive regime in which the reaction kinetics is first order in ρ_o. Although the crossover time scale for this transition does not agree with theoretical predictions, we find that a layer where the reactants are depleted develops near the interface on a time scale, τ_p consistent with theoretical predictions for the crossover time from the second to first-order reaction kinetics.

We found that $\Sigma(t)$ is independent of the chain length for these times and depends only on ρ_o for $t < \tau_g$. This is because $\Sigma(t)$ only depends on the chain end displacement $x(t)$ which is independent of Z for $t < \tau_g$. However, the scaling form for $t < \tau_g$ is different from what is expected. We found that $\Sigma(t)$ can be written in the scaling form $\Sigma(t) = g(t(\rho_o a^3)^3)$ for a wide range of ρ_o. This implies that, for this range of ρ_o, there is an additional crossover time scale which behaves as ρ_o^{-3} which has not been predicted theoretically. We argued, however, that this scaling must break down for very large and very small ρ_o.

Although the early time behavior ($t < \tau_p$) of $\Sigma(t)$ shows a trend toward a theoretically predicted linear growth regime at very small ρ_o, we cannot obtain the linear growth regime directly. As an alternative, we introduced a dilute limit model in which we keep track of number of unique pairs of chain ends that approach each other without actually linking the chains on approach. Using this model, we are able to measure the reaction constant in the dilute limit and we find that the linear reaction rate K_o is a slowly decreasing function of Z in qualitative agreement with the theoretical prediction that $K_o \sim 1/\ln Z$. A quantitative comparison also shows reasonable agreement for the longer chains in our simulations. The dilute limit model also agrees with the theoretical prediction of a logarithmic correction to the linear growth for times less than τ_g.

The interface is unstable and develops corrugations at later times for sufficiently large ρ_o. By measuring the surface tension as a function of time, we find that the surface tension vanishes before the interface becomes unstable. Hence, the interfacial instability is driven mainly by the vanishing surface tension rather than additional kinetic mechanisms. We find that the time τ_σ required for the surface tension to vanish scales as $\tau_\sigma \sim \rho_o^{-3}$ for the range of ρ_o that we studied.

Acknowledgment. We would like to thank A. C. Shi, D. Jasnow, and A. C. Balasz for helpful comments. We would also like to thank Scott Smith for his help in getting the computers working. Finally we gratefully acknowledge the support of the National Science Foundation through NSF Grant DMR-9986879.

References and Notes

(1) Manson, J. A.; Sperling, L. H. *Polymer Blends and Composites*; Plenum Press: New York, 1976.

(2) *Polymer Blends*, Paul, D. R., Newman, S., Eds.; Academic Press: New York, 1978.
(3) Utracki, L. *Polymer Alloys and Blends*; Hanser: New York, 1989.
(4) Utracki, L. A. *Polym. Networks Blends* **1991**, *1*, 61.
(5) Koo, K.-K.; Inoue, T.; Miyasaka, K. *Polym. Eng. Sci.* **1985**, *25*, 741.
(6) Rätzsch, M. *Makromol. Chem. Macromol. Symp.* **1987**, *12*, 165.
(7) Brown, S. B. *Annu. Rev. Mater. Sci.* **1991**, *21*, 409.
(8) Nishio, T.; Suzuki, Y.; Kojima, K.; Kakugo, M. J. *Polym. Eng.* **1991**, *10*, 123.
(9) P. Guégan, P.; Macosko, C. W.; Ishizone, T.; Hirao, A.; Nakahama, S. *Macromolecules* **1994**, *27*, 4993.
(10) Noolandi, J.; Hong, K. M. *Macromolecules* **1982**, *15*, 482.
(11) Leibler, L. *Makromol. Chem., Macromol. Symp.* **1988***16*, 1.
(12) Wang, Z. G.; Safran, S. A. *J. Phys. (Paris)* **1990**, *51*, 185.
(13) Shull, K. R.; Kellock, A. J.; Deline, V. R.; MacDonald, S. A. *J. Chem. Phys.* **1992**, *97*, 2095.
(14) Sundararaj, U.; Macosko, C. W. *Macromolecules* **1995**, *28*, 2647.
(15) Milner, S. T.; Xi, H. *J. Rheol.* **1996**, *40*, 663.
(16) Orr, C. A.; Adedeji, A.; Hirao, A.; Bates, F. S.; Macosko, C. W. *Macromolecules* **1997**, *30*, 1243.
(17) Lyu, S. P.; Cernohous, J. J.; Bates, F. S.; Macosko, C. W. *Macromolecules* **1999**, *32*, 106.
(18) Jiao, J.; Kramer, E. J.; de Vos, S.; Möller, M.; Koning, C. *Polymer* **1999**, *40*, 3585.
(19) O'Shaughnessy, B.; Sawhney, U. *Phys. Rev. Lett.* **1996**, *76*, 3444.
(20) O'Shaughnessy, B.; Sawhney, U. *Macromolecules* **1996**, *29*, 7230.
(21) Fredrickson, G. H. *Phys. Rev. Lett.* **1996**, *76*, 3440.
(22) Fredrickson, G. H.; Milner, S. T. *Macromolecules* **1996**, *29*, 7386.
(23) O'Shaughnessy, B.; Vavylonis, D. *Europhys. Lett.* **1999**, *45*, 638.
(24) O'Shaughnessy, B.; Vavylonis, D. *Macromolecules* **1999**, *32*, 1785.
(25) B. O'Shaughnessy, B.; Vavylonis, D. *Phys. Rev. Lett.* **2000**, *84*, 3193.
(26) Kramer, E. J. *Isr. J. Chem.* **1995**, *35*, 49.
(27) Oyama, H. T.; Inoue, T. *Macromolecules* **2001***34*, 5551.
(28) Oyama, H. T.; Ougizawa, T.; Inoue, T.; Weber, M.; Tamaru, K. *Macromolecules* **2001***34*, 7017.
(29) Müller, M. *Macromolecules* **1997**, *30*, 6353.
(30) Yang, Y.; Char, K. *Macromol. Theory Simul.* **2001**, *10*, 565.
(31) Kremer, K.; Grest, G. S. *J. Chem. Phys.* **1990**, *92*, 5057.
(32) Grest, G. S.; Kremer, K.; Duering, E. R. *Europhys. Lett.* **1992**, *19*, 195.
(33) Grest, G. S.; Kremer, K.; Duering, E. R. *Physica A* **1993**, *194*, 330.
(34) Grest, G. S.; Lacasse, M.-D.; Kremer, K.; Gupta, A. M. *J. Chem. Phys.* **1996**, *105*, 10583.
(35) Lacasse, M.-D.; Grest, G. S.; Levine, A. J. *Phys. Rev. Lett.* **1998***80*, 309.
(36) Murat, M.; Grest, G. S.; K. Kremer, K. *Europhys. Lett.* **1998**, *42*, 401.

MA021229X